Hemispherical Reflectance and Emittance Properties of Carbon Nanotubes Coatings at Far-Infrared Wavelengths

Manuel A. Quijada, John G. Hagopian, Stephanie Getty, Raymond (Robin) E. Kinzer, Jr., and Edward Wollack

Goddard Space Flight Center, 8800 Greenbelt Rd., Greenbelt, MD 20771;

ABSTRACT

Recent visible wavelength observations of Multiwalled Carbon Nanotubes (MWCNT) coatings have revealed that they represent the blackest materials known in nature with a Total Hemispherical Reflectance (THR) less than 0.25%. This makes them as exceptionally good absorbers, with the potential to provide order-of-magnitude improvement in stray-light suppression over current black surface treatments when used in an optical system. Here we extend the characterization of this class of materials into the infrared spectral region to further evaluate their potential for use on instrument baffles for stray-light suppression and to manage spacecraft thermal properties to dissipate heat through radiant heat transfer process. These characterizations will include the wavelength-dependent Total Hemispherical Reflectance properties in the mid-IR and far-infrared spectral regions (2-100 μm). Determination of the temperature-dependent emittance will be investigated in the temperature range of 20 to 300 K. These results will be compared against other more conventional black coatings such as Acktar Fractal Black or Z-306 coatings among others.

Keywords: Multi-Walled Carbon Nanotubes (MWCNT), Hemispherical Reflectance, Emittance, Stray-light.

1. INTRODUCTION

There has been an active program NASA Goddard Space Flight Center (GSFC) Internal Research and Development (IRAD) program "Nanostructures for Stray Light and Diffraction Suppression," (J.G.Hagopian PI), researching carbon nanotubes since 2007. Our group has found that Multiwalled Carbon Nanotubes (MWCNTs) are exceptionally good absorbers, with potential to provide order-of-magnitude improvement over current surface treatments and a resulting factor of 10,000 reduction in stray light when applied to an entire optical train.[1] The research has been motivated by the stringent stray light control needs which occur in the realization of precision optical systems for remote sensing. Examples include Earth observations by satellite imaging systems where high brightness contrast exists between desired field of view and other backgrounds sources which can illuminate and scatter from elements of the instrument. This bright light diffracts from instrument structures, rattles around and invariably contaminates measurements. Astrophysical observations also are impacted by stray light that obscures very dim objects and degrades signal to noise in spectroscopic measurements. Stray light is controlled by utilizing low reflectance structural surface treatments and by using baffles and stops to limit this background noise. Development of this technology will provide numerous benefits including the increase in observational efficiencies by recovering currently unusable scenes in high contrast regions.[2]

Our objective has been to develop and apply MWCNTs to instrument components to realize the benefits mentioned above. We have addressed the technical challenges to advance the technology by tuning the MWCNT growth geometry using a variety of methods and on various types of substrates to provide a factor of 10 improvement in absorption in the near UV, visible and near-infrared spectral ranges over current surface treatments used in space flight hardware.[1] Hence, the purpose of this paper is to explore the potential of MWCNT as thermal-control coatings at mid- and far-infrared wavelengths by reporting characterization of the Total Hemispherical Reflectance (THR) in the 0.2 to 100 μm. These results will be extended to different types of MWCNT samples grown on different substrates. They will be used to derive the wavelength-dependent and total emittance

Further author information: (Send correspondence to M.A.Q.)
M.A.Q.: E-mail: manuel.a.quijada@nasa.gov, Telephone: 1 301 286 3544

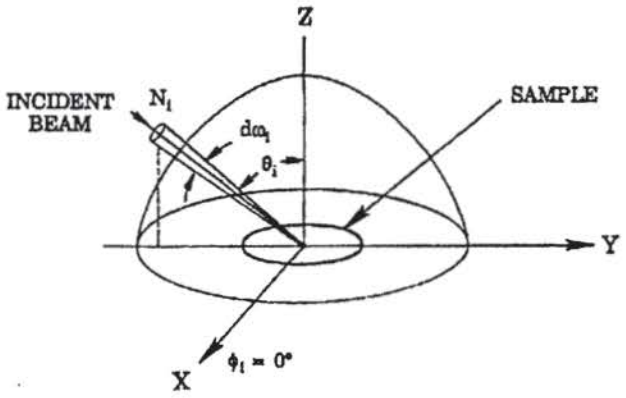

Figure 1. Diagram illustrating concept of directional reflectance.

properties as a function of temperature. We have used this type of characterization to optimize the growth process and geometry for robustness and maximum absorption. In addition to the applications mentioned above optimization of the MWCNT samples will be pursued in detector applications to enhance light absorption and quantum efficiency. The paper is organized as follows. We will first present a discussion of the hemispherical reflectance properties and the equipment used to measure this quantity in all of our samples. We will then proceed to a description of the method used to derive the temperature dependence in the total emittance. This will be followed by a description optimization in the growth process of the MWCNT samples on various types of substrates. We will then proceed to show the results obtained from these samples. The paper will end with some concluding remarks.

2. REFLECTANCE PROPERTIES

2.1 Directional Reflectance

The directional reflectance (DR) of a surface is defined as the ratio of the total energy reflected into the subtending hemisphere to the energy incident (N_i) on the surface from the direction θ_i, ϕ_i (see Fig. 1). Following the notation of Nicodemus,[3] the directional reflectance may be expressed in terms of primary quantities as

$$\rho_d(\theta_i, \phi_i) = \frac{\int_0^{2\pi} \int_0^{\pi/2} N_r \sin\theta_r \cos\theta_r \, d\theta_r \, d\phi_r}{N_i \sin\theta_i \cos\theta_i \, d\theta_i \, d\phi_i} \tag{1}$$

The relation between directional and bidirectional reflectance (BDR) is given by the integral of the latter over the viewing hemisphere

$$\rho_d(\theta_i, \phi_i) = \int_0^{2\pi} \int_0^{\pi/2} \rho'(\theta_i, \phi_i; \theta_r, \phi_r) \sin\theta_r \cos\theta_r \, d\theta_r \, d\phi_r \tag{2}$$

For a perfectly diffuse isotropic reflector ($\rho'(\theta_i, \phi_i; \theta_r, \phi_r) = constant$), integration of Eq. 2 gives

$$\rho_d = \pi\rho' \tag{3}$$

2.2 Quantities Derived from Reflectance Properties

The measured directional reflectance of a sample may be used to compute two important properties required for radiative heat transfer analysis, e.g., the directional emittance and the solar absorptance.

2.2.1 Emittance

By reasons of conservation of energy, the directional emittance of an opaque surface at a given wavelength and angle of incidence may be expressed by

$$\varepsilon_d(\theta_i, \phi_i, \lambda) = 1 - \rho_d(\theta_i, \phi_i, \lambda), \tag{4}$$

or for transmissive surfaces

$$\varepsilon_d = 1 - (\rho_d + T_s), \tag{5}$$

where $\rho_d(\theta_i, \phi_i, \lambda)$ and T_s are the measured directional reflectance and transmittance respectively. We will drop the θ_i and ϕ_i dependence of ρ_d and ε_d for reasons of brevity for the remaining discussion. From the relations in Equations (4) and (5), the total directional emittance of the surface at a given temperature may be found by

$$\varepsilon_t(\theta_i, \phi_i, \lambda) = 1 - \frac{\int_0^\infty \rho_d(\lambda) P(\lambda, T) d\lambda}{\int_0^\infty P(\lambda, T) d\lambda} \tag{6}$$

or for transmissive surfaces

$$\varepsilon_t(\theta_i, \phi_i, \lambda) = 1 - \frac{\int_0^\infty (\rho_d + T_s) P(\lambda, T) d\lambda}{\int_0^\infty P(\lambda, T) d\lambda} \tag{7}$$

where

$$P(\lambda, T) = \frac{8\pi hc}{\lambda^5 (e^{hc/\lambda T k} - 1)} \tag{8}$$

is Planck's Function for the given wavelength (λ) and temperature (T). Substituting values for the Planck's constant h, speed of light c and Boltzman constant k and providing the appropriate unit conversion so λ can be expressed in μm we get

$$P(\lambda, T) = \frac{0.000119088}{\lambda^5 [e^{14388/\lambda T} - 1]} \tag{9}$$

The equations above allow emittance determination in various instances depending on the angular coverage of the reflectance measurements. The first instance is directional angular emittance when reflectance is measured at any angle of incidence including near-normal ($\theta \leq 10°$) reflectance. The second case is spectral hemispherical emittance $\varepsilon_H(\lambda)$, when reflectance has been measured over a sufficiently wide range of incidence angles to permit integration overall the hemisphere, i.e.:

$$(\varepsilon_H) = 1 - 2 \int_0^{\pi/2} \rho_d(\lambda) \sin\theta \cos\theta \, d\theta. \tag{10}$$

Finally, total hemispherical emittance (ε_H), when reflectance has been measured over a sufficiently wide range of incidence angles to permit integration over the hemisphere,

$$\varepsilon_H = 2 \int_0^{\pi/2} \varepsilon_t(\theta) \sin\theta \cos\theta \, d\theta. \tag{11}$$

2.3 Total Hemispherical Reflectance

For specular reflectance, the angle of reflection is equal to the angle of incidence on the substrate; direct reflection off the surface is carefully controlled. In most optical instruments the source of stray light that is more difficult to control is the scattered light at all angles. This light can be reflected many times and find its way to the instrument focal plane where it can degrade the observations by creating noise that obscures the signal of interest. Characterization of this scattered light leads us to the concept of Total Hemispherical Reflectance (THR) which is the reflectance measured of all light that is scattered off of a test sample at all angles. The measurement of THR does not discriminate the angle of reflectance only the total amount of reflected light. It is also a good measure of the relative ability of materials to absorb light and therefore it could be an effective screening tool to

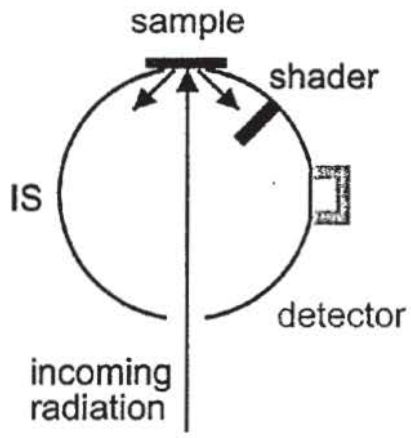

Figure 2. Illustration of integrating sphere for hemispherical reflectance measurements.

determine the effectiveness of a particular MWCNT growth process. It does not however provide the full range of characterization required for modeling an instrument to determine system stray light.

The THR measurements invariably require the use of an integrating sphere in a configuration as shown in Fig.2. This diagram shows the incoming beam illuminates the test sample from a given direction and the radiation scattered by the sample is collected and detected. The results reported here on the MWCNT samples were done over a spectral range from 0.2 to 100 μm. Collection of data over such a wide range required the use of up to 3 instruments. The UV/Vis/NIR spectral range included from 0.2 to 2.5 μm was done with a Perkin Elmer Lambda 950 equipped with a 60 mm integrating sphere. The light detection is done by two detectors located inside the sphere: A lead sulfide (PbS) detector to cover the 0.860-2.500 μm and a R955 photomultiplier tube (PMT) for the wavelength range between 0.200 and 0.860 μm. Finally the inside of the sphere is coated with a spectralon coating.

For coverage at longer wavelengths, we used a Bruker Fourier Transform Infrared (FTS) spectrometer (IFS 125HR) with an integrating sphere accessory. A second Bruker FTS spectrometer (IFS 113) equipped with a reflectometer that is capable of providing THR data from 20 to 100 μm. In addition, this instrument has the capability of provide measurements at cryogenic temperatures (5 to 100 K). Operational features and construction details for all these instruments will be provide in the following sections.

2.4 Bruker FTS Integrating Sphere Reflectometer

The Bruker IFS125 was the instrument of choice to collect data in the 2 to 25 μm spectral range at ambient temperature (300K). Adequate experimental conditions for measurements in this spectral range were achieved by choosing combinations of the following components: tungsten lamp or glow-bar source, Si/CaF2 or Ge/KBr beam splitter and a DTGS detector. The reflectance attachment that went along these measurements was mounted in the sample compartment of the spectrometer and consists of a hollow sphere (75mm diameter) coated with an electro-deposited Lambertian gold coating on the inside. As the Fig. 3 shows, the sphere has one beam inlet port, two sample ports and one outlet port allowing the light to reach the detector after the integration. The infrared (IR) beam enters the integrating sphere through the beam inlet pot and impinges on the beam-steering mirror which is mounted inside the sphere slightly off center. Depending on the position of the beam-steering mirror, the IR-beam is directed either to the upper or lower sample port. In either case the angle of incidence for the IR beam impinging on the sample (or reference)is 13°. In this configuration, the specularly as well as the diffusely reflected radiation hit the sphere wall at least once and therefore both are included in the flux measurements. In this arrangement no baffles are needed.

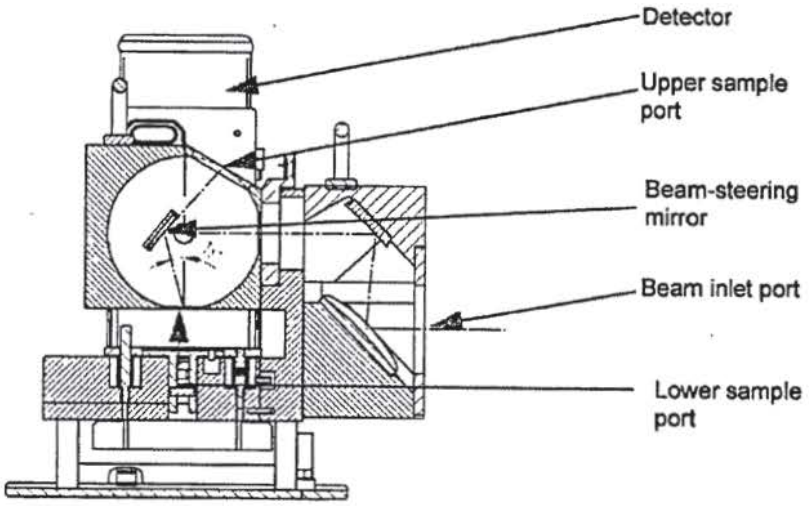

Figure 3. Diagram of the Bruker IFS125 integrating sphere reflectometer.

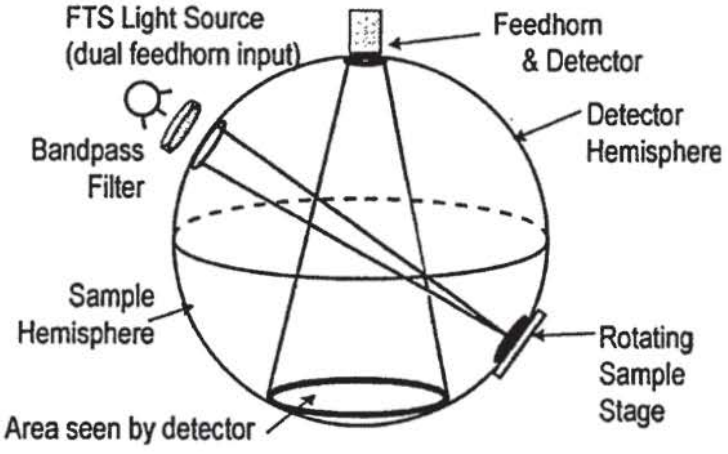

Figure 4. Diagram of the Opasi-T cryo-reflectometer.

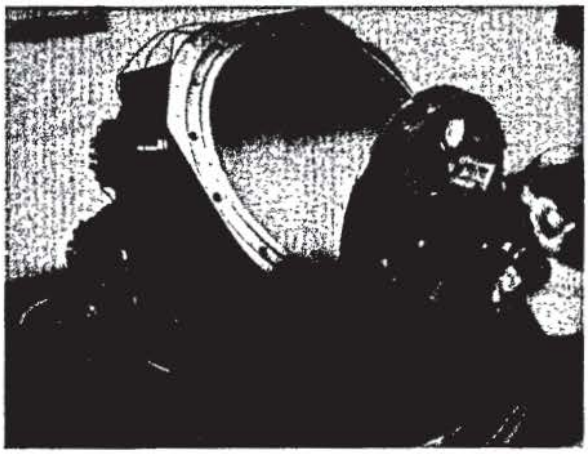

Figure 5. Picture of gold-coated OPASI-T cryo-reflectometer integrating sphere.

2.5 OPASI-T Cryo-Reflectometer

For measurements in the Far-infrared spectral region (20 to 100 μm) we used a reflectometer fitted to Bruker IFS 113 spectrometer. This system is specifically designed for performing Hemispherical reflectance at cryogenic temperatures. This system was originally designed and constructed to be used in the Optical Properties of Astronomical Silicates with Infrared Techniques (OPASI-T) program.[4] The purpose of this custom FTS accessory was to characterize the diffused reflectance of astronomical dust particulate analogs as a function of concentration. Figure 4 shows a diagram of the reflectometer that is fitted with an integrating sphere to provide measurements for wavelengths larger than 15 μm and at temperatures between 5 and 100 K. The integrating sphere itself is machined aluminum; the interior surface of the sphere is bead blasted with 16-grit silicon carbide, creating an approximately isotropic scattering surface, and gold-plated to maximize surface reflectivity (see Fig. 5). Light enters the sphere through a double-ended f/6 Winston cone; this provides illumination to a small patch (21.8 mm diameter) on the target. The input light is either a mercury arc or a glow-bar that comes from inside the Bruker IFS 113 v FTS. Three targets sit within a three-position sample wheel, allowing us to measure in sequence a black (absorptive) target, a reflective target, and the test sample. The wheel also has a magnetic switch that allows accurate tracking of the rotation position. Light reflected off this test sample then scatters inside the sphere to an f/2.44 Winston cone that brings the light to an IR Labs cooled germanium bolometer. This cone is positioned so that light from the sample cannot directly reflect from the sample into the detector Winston cone; this eliminates the need for baffling inside the sphere. The sphere and bolometer are mounted to the cold plate of a liquid Helium cryostat. The sample wheel is thermally isolated from the cold plate with a stainless steel support bracket, with a mechanical heat switch to provide the ability to thermalize the wheel. Mounted to the wheel are both a thermometer and a 300 Ω resistive heater; the heater allows the wheel, when isolated, to be temperature controlled between $\simeq 4.2$ K and ~ 100 K. Thermal radiation from the wheel provides the limit at the upper end of this scale, as when the wheel temperature exceeds 100 K, it radiatively heats the bolometer.

3. MWCNT GROWTH AND OPTIMIZATION

The growth of high-absorption low hemispherical reflectance MWCNT samples has been achieved through 3 phases. The effort during the first phase consisted of tuning the nanotube geometry to produce the desired low reflectance over all angles on silicon. Next we worked on improving adherence of the MWCNT layers onto silicon. Finally, we have worked on nanotubes deposition on alternate substrates in order to broaden the scope of application, such as improved components for stray light suppression and enhancing quantum efficiency of infrared detector absorbers.

3.1 MWCNT Growth on Silicon

Fabrication of vertically oriented MWCNT films was accomplished by catalyst-assisted chemical vapor deposition (CVD). Using silicon as the growth substrate, the fabrication begins with the thermal deposition of aluminum/iron thin film catalyst. To grow MWCNTs, the substrate is exposed to ethylene feedstock gas at 750 °C in a reducing environment; the ethylene is dissociated at the iron surface, and the carbon is extruded in the form of a dense film of aligned MWCNTs. Precise patterning of the MWCNT film can be accomplished by constraining the placement of the catalyst film through conventional lithographic means. Varying the catalyst thickness on the substrate can modulate the MWCNT height. We also used the modulation of catalyst film thickness to produce low-density, tall MWCNTs. We studied the extreme regime of catalyst thickness to characterize the limits of this technique to producing low MWCNT fill factors. Minimization of catalyst film thickness resulted in an order of magnitude improvement in the performance of the MWCNT as an absorber. Our process resulted in multiwalled carbon nanotubes with inner diameters of 1-5 nm, outer diameters of 30-100 nm and average spacing of 100-500 nm. The best samples had lengths of 50 to 100 *mum*, but it is highly probable that longer lengths would provide better performance.[2] In addition this being one of our active areas of research, we have also recognized the importance of carbon nanotube adhesion given the environmental conditions associated with end usage. Other properties we have considered are how straight the fibers lie, their heat capacity, charging properties in a radiation environment and others. The adhesion question is discussed in more detail in the following section.

3.2 Adhesion enhancement on silicon

Carbon nanotubes grown on silicon with only the iron catalyst layer exhibit poor adhesion; it is quite easy to rub the nanotubes off of the substrate with any contact. This poor adhesion severely limits the utilization of MWCNTs in space flight hardware. Previous work suggests that the point of failure is at the catalyst-substrate interface. We explored alternative substrate preparation techniques to improve adhesion. The primary approach we developed was the use of a thin-film sticking layer under the iron catalyst layer. We experimented with chromium, titanium and alumina underlayers. The approach was straightforward and should not have significantly impacted the favorable properties of the thin Fe catalyst film. What we found however was that the nanotube growth properties were significantly affected by this layer. After much trial and error, it was determined that alumina provided a good sticking layer without degrading the optical properties of the carbon nanotubes.

3.3 Growth on alternate materials

As mentioned above, the nanotubes films are typically grown on silicon substrate. Although many optical components including mirrors, slits and small blocking elements such as coronographic masks could be feasibly made out of silicon, the use of this substrate alone will limit the usability of the nanotube coatings in situations where it is required to use more robust substrates. We investigated and determined a growth process that yielded similar performance as samples grown on silicon. The substrates investigated included stainless steel, nickel and titanium using the same thickness of iron catalyst layer and growth parameters optimized on the silicon substrates. Titanium substrates produced excellent performance when the adhesion layer thickness was increased. Successful growth using the optimized process was also achieved on stainless steel. In addition, growth on silicon nitride (SiN) is an active area of research at GSFC given that SiN membranes with nanotubes have a great potential to be used as infrared detector absorber structures. Further optimization of the reflective properties was performed by varying the surface substrate roughness, varying the time of hydrogen introduction prior to growth and varying the thickness of the catalyst layer.

4. RESULTS

4.1 THR Reflectance at Ambient Temperature

Figure 6 shows THR data for several nanotube samples grown of different substrates. The sample with the highest THR values in the short wavelength range (below 2 μm) is the one labeled "1mm long". This is a sample that was grown at Southern Illinois University (by Saikat Talapatra) that was initially determined to have poor performance in the UV-NIR. Measurements in the Mid-Infrared show however that they become much better

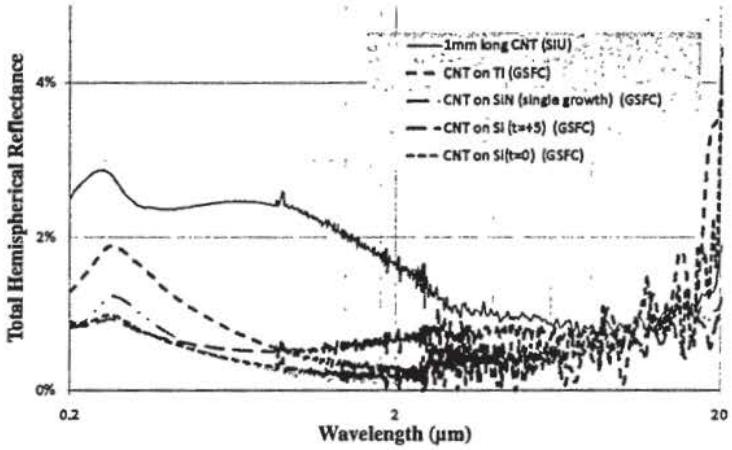

Figure 6. Carbon nanotube hemispherical reflectance for a variety of substrates.

absorbers in this region. The silicon substrate, silicon nitrate and titanium substrate samples all have nanotube lengths of 50 to 100 μm. Hence, the results in Fig. 6 show that they all perform better in the Near UV-NIR but are similar to the "1mm long" sample at longer wavelengths. This is probably due to the difference in the effective index of refraction of the samples as a function of wavelength. The initial interaction of light with the nanotube mat results in reflection based on the "effective" index change between air (or vacuum) and the nanotubes. Since carbon has a relatively high index, we want a very low density of nanotubes so that the boundary does not produce a large reflection. Bulk carbon is black but very shiny due to its high index. The nanotube mat has about a 1% fill factor making the effective index approach 1 to prevent a high impedance mismatch. The density of the "1mm long" sample is higher, therefore it reflects more light at short wavelengths. At longer wavelengths, the index changes similarly for all samples, but the penetration of the light into the nanotube mat begins to dominate, with a higher efficiency of absorption for the taller mats. Therefore, best performance requires an optimization of density and height to provide best broad band absorption. Finally, we show two samples grown on silicon with the growth parameter "t being the time of hydrogen pre-treat before growth" set at "t=0" and "t=+5". The "t=0" sample is the one with the lowest THR of all the samples measured and shown in Fig. 6.

4.2 Far-Infrared Cryo-Reflectance

We now turn our attention to hemispherical reflectance obtained with the OPASI-T reflectometer on three selected samples from the set shown in Fig 6. But before we do this, lets first discuss the procedure by which these data are obtained. In a typical experiment, the wheel in the reflectometer is first set on a position that has a highly reflecting surface of either Au or Al. A series of scans are measured and consecutive ratios are taken to establish the point at which the whole system including the LHe cooled bolometer detector have reached a steady state thermal equilibrium. This condition is reached when those ratios give a nearly constant 100% curve, as it is the case for the curve labeled "100%baseline" in Fig. 7. Once the system has been deemed stable, a series of 100% baseline single beam spectra are collected and averaged. After this, the filter wheel is rotated to the position of the "black" calibrator to collect the 0% baseline single beam spectra. This "black" calibrator, a figure of which is shown in Fig. 8, has a regularly textured surface that has been specifically engineered to create a "rough surface" to help make it black at far-infrared wavelengths.[5,6] In addition, the surface is coated with an highly absorbing layer of Actar Fractal Black to provide the maximum absorption possible in the Far- and Mid-infrared spectral regions. These data are shown in Fig. 7 with the curve labeled "0%baseline" that is the ratio of the "black" single beam data to that of the 100% reference collected earlier. We observe this ratio has an average value close to 62%. Ideally, one would have expected this ratio to be much smaller than that, as the hemispherical reflectance for this "black" sample has been independently verified to be around 1-2% in this wavelength range. However, this is not the case here due to the fact that the sample is being illuminated by a roughly 30% oversized beam. Hence, most of this signal results from reflected light that also hits a Al mask

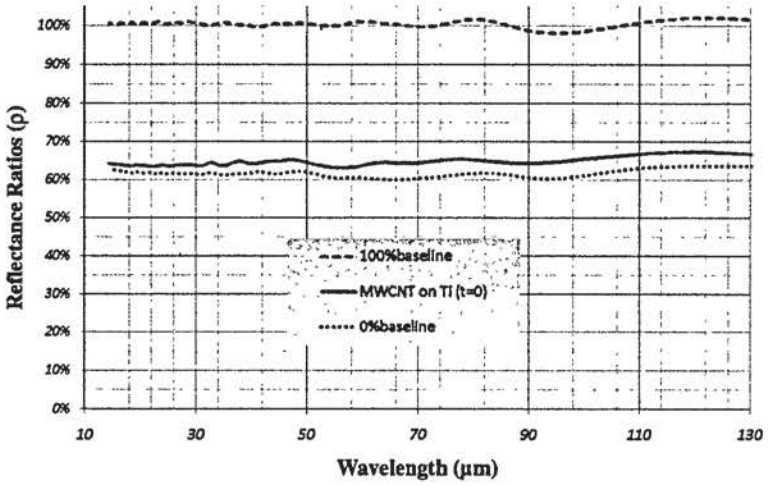

Figure 7. Reflectance ratios of the "black" calibrator and a MWCNT sample grown on Ti relative to the 100% reference sample. Note: The dashed blue line corresponds to the ratio of two consecutive 100% baseline single-beam spectra to demonstrate the system estability.

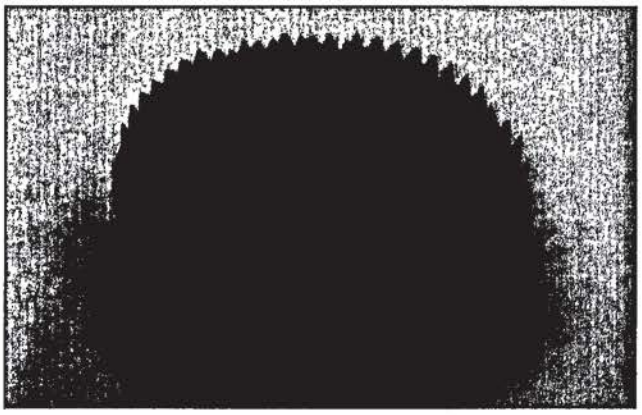

Figure 8. Image of aluminum substrate disk with a regularly texture surface. This device is used as our "black" standard to provide 0% baseline spectral calibration. Notice also device is shown before coating with Actar Fractal black coating is applied. Once coated, the structure details of this standard are difficult to see

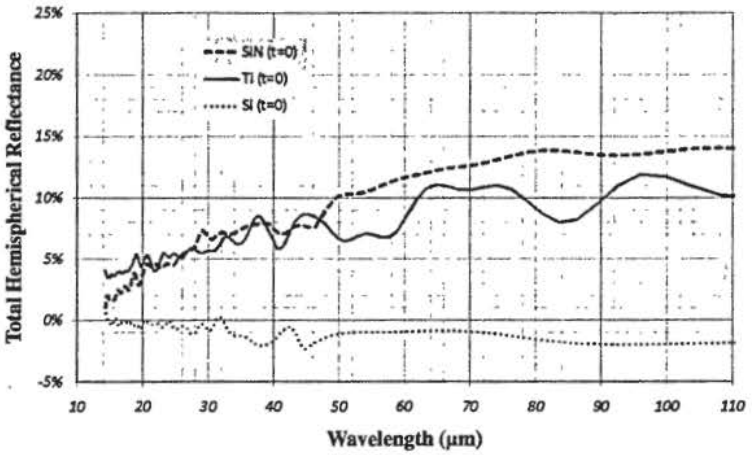

Figure 9. Total Hemispherical Reflectance for three MWCNT samples grown on Si, SiN and Ti substrates.

with a square opening in the middle of roughly $\simeq 1\times1$ cm^2 dimensions. The size for this center opening was determined by the typical size of the MWCNT's used for these tests. This leads us to the last data set labeled "MWCNT on Ti(t=0)" in Fig. 7 which corresponds to measurements on a MWCNT sample grown on titanium substrate. This ratio is calculated from the single beam spectra of this sample to that of the 100% reference sample. The average value is around 64% and this suggests that in this case the MWCNT sample is slightly more reflecting that the 0% reference black sample. The final step in order to obtain properly normalized THR data from these ratios (ρ) is done by means of the formula:

$$R_H = \frac{\rho_{sample} - \rho_{0\%baseline}}{\rho_{100\%baseline} - \rho_{0\%baseline}} \tag{12}$$

The results of applying the calculations of Eq. 12 to the data in Fig. 7, along with results obtained on two more samples grown on Si and SiN substrates are shown in Fig. 9. The THR values for all the samples start off in agreement with the $\lambda \sim 20\mu$m data shown in Fig. 6. However, the data for both Ti and SiN samples show a positive (almost linear) increase towards longer wavelengths, reaching values near 10% and 14% for each samples respectively at the high-end wavelengths. This suggests that the these coatings are becoming less effective in absorbing electromagnetic radiations at longer wavelengths. This is in contrast with the Si sample where the THR values start near zero, and actually turn negative when the calculations are done using the definition given in Eq. 12. This simply means the MWCNT Si sample is actually a better absorber (or lower reflector) than our "black" calibrator. This is quite remarkable given all the effort that went into the design and fabrication of this device.[7] The fact that the Si sample is a better performer in terms of low THR at Far-Infrared wavelengths is not surprising. This may suggest this sample may have longer and/or better aligned nanotubes when compared to either the SiN or Ti sample.

4.3 Emittance Calculations

We now turn our attention to calculating emittance versus temperature using the equations presented in Sec. 2.2.1. We performed these calculations for the three samples shown in Fig. 9. We also compare these results with other more traditional black coatings. These results are shown in Fig. 10. The integral in Eq. 7 implies that the THR data would be needed over an infinite wavelength range. But in practice, it is only sufficient that the THR data extend over the temperature range where the Plank's function would make an appreciable contribution to the integral in Eq. 7. For example, the maximum for the Planck's function lies at 97 μm at a temperature of 30K, whereas the maximum shifts to 10 μm at a temperature of 300K. Another important consideration is that the measured THR does not have a strong dependence on temperature. We have validated

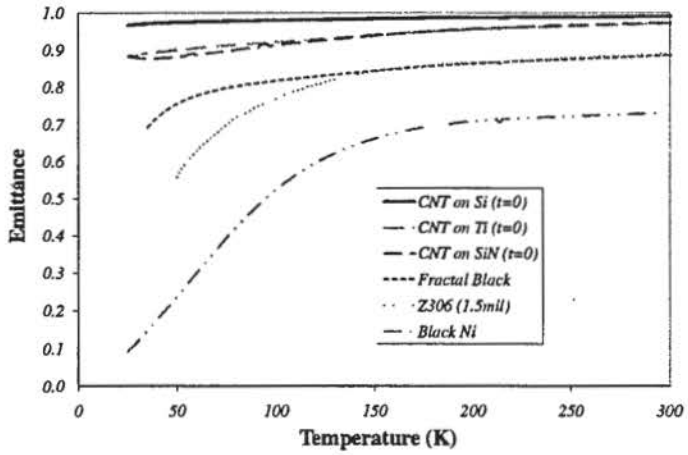

Figure 10. Temperature-dependent emittance for various black paints.

this assumption in the present case since we found the THR data at ambient (300K) temperature merge smoothly without any discontinuity in the range they overlap with the far-infrared data taken at 5K on the same sample.

The results of this analysis yields an integrated emittance that is the highest for the CNT grown on silicon (Si(t=0)) substrate. The average value of $\varepsilon(T)$ stays around 97-98% over the range of temperature shown in Fig. 10. The carbon nanotubes coating grown on Ti and SiN display the second and third best emittance values as a function of temperature (average values over 95% for both samples). These averages compare favorably with the current state-of-the-art that are typically measured on Fractal black and other more commonly used black paints such as Z306.

5. CONCLUSIONS

In conclusion, we have performed Total Hemispherical Reflectance measurements on Multiwalled Carbon Nanotube samples grown on a various substrates in the visible mid- and far-Infrared wavelengths. These results show that samples prepared on Si substrate display the lowest THR value ever recorded across a very broad spectral range (0.2 to 110 μm). Furthermore, samples grown on Ti or SiN offer comparable performance but only up to 20 μm. The THR for these are substantially higher at wavelengths as long as 110 μm, when compared to the Si-based sample. This may suggest the carbon nanotubes may not be as long or better aligned as they are on the Si based samples. These data lead to the highest emittance value ever reported for a black coating at infrared frequencies all the the way down to 30-40 K.

ACKNOWLEDGMENTS

This work is supported through a NASA-Goddard Space Flight Center (GSFC) Internal Research and Development (IRAD) grant. One of us, Raymond (Robin) E. Kinzer Jr., is supported by an appointment to the NASA Postdoctoral Program at GSFC administered by the Oak Ridge Associated Universities under contract with NASA.

REFERENCES

[1] John G. Hagopian, Stephanie A. Getty, Manuel Quijada, June Tveekrem, Ron Shiri, Patrick Roman, James Butler, Georgi Georgiev, Jeff Livas, Cleophus Hunt, Alejandro Maldonado, "Multiwalled carbon nanotubes for stray light suppression in space flight instruments," *Proc. SPIE* **7761**, 77610F (2010).

[2] Zu-Po Yang, Lijie Ci, James A. Bur, Shawn-Yu Lin, and Pulickel M. Ajayan, "Experimental observation of an extremely dark material made by a low-density nanotube array," *Nanoletters* **8**, 446–451 (2007).

[3] Nicodemus, F. E., Richmond, J. C., Hsia, J. J., Ginsberg, I. W., and Limperis T., [*Geometrical considerations and nomenclature for reflectance*], National Bureau of Standards Monograph 160, US Department of Commerce, Washington (1977).

[4] Stephen A. Rinehart, Dominic J. Benford,1 Giuseppe Cataldo, Eliahu Dwek, Ross Henry, Raymond E. Kinzer, Jr., Joseph Nuth,3 Robert Silverberg, Caleb Wheeler, and Edward Wollack, "Measuring the optical properties of astrophysical dust analogues: instrumentation and methods," *Applied Optics* **50**, 4115–4124 (2011).

[5] E.J. Wollack, D.J. Fixsen, A. Kogut, M. Limon, P. Mirel, J. Singal, "Radiometric waveguide calibrators," *IEEE Transactions on Instrumentation and Measurement* **56**, 2073–2078 (2007).

[6] D.J. Fixsen, E.J. Wollack, A. Kogut, M. Limon, P. Mirel, J. Singal, J., "Compact radiometric microwave calibrator," *Review of Scientific Instruments* **77**, 64905–1–6 (2006).

[7] J.R. Eimer, C.L. Bennett, D.T. Chuss, E.J. Wollack, "Precision reflectometry in a beam waveguide," *Review of Scientific Instruments* **82**, 086101–4 (2011).